PORE-SCALE TO CORE-SCALE STUDY OF CAPILLARY DESATURATION CURVES USING MULTI-SCALE 3D IMAGING

Rezki Oughanem[1,2], Souhail Youssef[1], Yannick Peysson[1], Brigitte Bazin[1], Eric Maire[2], Olga Vizika[1]

[1]IFP Energies nouvelles, [2] INSA-Lyon MATEIS CNRS UMR 5510,

This paper was prepared for presentation at the International Symposium of the Society of Core Analysts held in Napa Valley, California, USA, 16-19 September, 2013.

ABSTRACT

The evolution of the residual oil saturation as function of the capillary number, ratio of viscous to capillary forces, is known as the Capillary Desaturation Curve (CDC) and constitutes an important input parameter in EOR reservoir simulations. In this work we present a new experimental workflow combined with pore-scale 3D imaging to investigate the effect of flooding parameters, fluid interfacial properties and rock structure on the CDC. Core flood experiments were combined with CT-scan imaging to accurately measure the mean residual oil saturation at different capillary number values as well as the local saturation distribution along the core plug. The CDC was measured on a set of water-wet sandstones with different petrophysical properties. The capillary number was varied by injecting a surfactant solution at different flow rates. Pore-scale structure of the rock and microscopic structure of the residual oil saturation were captured using high resolution micro-CT (MCT). Pore network structural properties where extracted from MCT images. Results show that CDC shape strongly depends on aspect ratio and throat size distributions of the pore network. Finally, the impact of the initial oil blob size distribution is discussed.

INTRODUCTION

During the primary recovery stage, oil is produced through different natural mechanisms, where underground pressure is sufficient to drive oil from the far field to the production well; 5-25 % of the oil originally in place is typically produced. When natural reservoir pressure becomes insufficient to push oil to surface and secondary recovery methods (gas and water injection) are applied to maintain the pressure, recovery factor can reach up to 10-55 % of original oil in place [1]. The major part of the remaining oil is trapped as disconnected phase (clusters and ganglia) under capillary forces [2]. These forces are strongly related to the geometry of pore network, the fluid-fluid properties (interfacial tension) and fluid-rock properties (wettability) [3]. Chemical EOR methods' objective is to decrease residual oil by changing trapping conditions such as rock wettability [4] or fluid-fluid interfacial tension. Surfactant injection is a chemical method targeting a better oil microscopic displacement efficiency by reducing the interfacial tension between

trapped oil and water. Capillary forces have to be compared to the displacing forces (viscous and gravity). Previous works [5-12] described the competition between capillary forces and displacing forces through two dimensionless numbers: the capillary number, defined as the ratio of viscous to capillary forces, and the Bond number, defined as the ratio of gravity to capillary forces. Even though there is consensus on the qualitative effect of capillary number on the residual oil saturation, a considerable dispersion is observed on measured CDC. In fact, challenging experimental issues have to be addressed to produce a relevant CDC, among which the variation of the capillary number over three to four decades and the accurate measurement of small variations of oil residual saturation. Nevertheless, it's obvious that part of the observed dispersion is due to pore network topology and pore scale geometric properties.

The effect of pore structure on CDC has been reported by several experimental and theoretical works. Dullien et al [13] have defined a structural difficulty index based on the pore-size distribution determined by mercury porosimetry and photomicrography, and they found that the residual oil saturation correlate with this index at identical displacement conditions. Stegemeier [3] and Zhou and Stenby [14] have simulated CDC using pore throat radii distribution evaluated using first drainage capillary pressure and correlation describing trapped oil population. Stegemeier has used the I-R curve [15] which correlates residual oil saturation with initial oil saturation while Zhou and Stenby have used an effective accessibility correlation determined by percolation theory. A good estimation of experimental CDC was obtained on few samples. However these tow approaches fail to take into account migration of trapped cluster and their interaction. Yet these pioneer works show the dependency of CDCs to two main structural parameters: the throat size distribution and the trapped cluster size which impacts the accessibility path of the flooding fluid.

In this study we present an experimental workflow to investigate the effect of rock structure on the CDC using multi-scale CT imaging [16]. First, we describe coreflood experiments conducted in a wide selection of water-wet sandstones. The capillary desaturation curves obtained at Darcy scale exhibit an important dispersion. In a second step, to understand this dispersion, MCT scan experiments were performed, and pore space structure and initial microscopic distributions of residual oil saturation were carefully mapped.

MATERIAL AND METHODS

Fluid and rock properties

The displacement experiments at core scale were conducted using potassium iodide brine (4 wt. %) and n-Decane. The two fluids had a significant x-ray absorption contrast, allowing a satisfactory estimation and visualization of two-phase saturations using CT scanner. The interfacial tension between the brine and n-Decane was 40 dyn/cm. Lower interfacial tension was obtained by adding 0.025 wt. % of sodium dodecyl benzene sulfate (SDBS) surfactant and 5 % of isobutyl alcohol (Isobutanol) to the brine phase. The role of isobutyl alcohol is to facilitate the solubility of the SDBS in the brine phase.

The low SDBS concentration was chosen to reduce the formation of oil in water emulsions during injection. The interfacial tension between n-Decane and surfactant solution, measured by spinning drop method, is 0.3 dyn/cm. This permitted to increase the capillary number by almost two orders of magnitude. The brine (resp. with surfactant) viscosity and density were 0.93 cP (resp. 1.11 cP) and 1.027 g/cm^3 (resp. 1.020 g/cm^3). The n-Decane viscosity and density were respectively 0.93 cP and 0.734 g/cm^3 at 22 °C.

Highly consolidated water-wet Berea, Bentheimer, Fontainebleau and Clashach sandstones were chosen for this study. These rocks are classified as clean sandstones. In the core flooding experiment, core plugs used are typically 8 cm in length and 3.3 cm in diameter. The cores were first coated with 8 mm thick epoxy resin (Devon-Mill Crusher Liner) and dried in an oven at 60 °C for 48 hours. To compute mean and local porosity, cores were weighed and CT-scanned dry and saturated with brine under vacuum conditions. Macroscopic petrophysical properties and dimension of cores are reported in Table 1. Figure 1 shows for the different samples normalized porosity profile ($\phi_i/<\phi>$) calculated from CT-scan data. It can be seen that porosity profile of Clashach CL2 and Fontainebleau FB2 are heterogeneous compared to Bentheimer BH1 and Berea BE1 samples.

Table 1. Petrophysical properties of the cores used in core flood experiments

Core type	L (mm)	PV (cc)	K_a (md)	ϕ (%)	FF	S_{wi} (%)
Berea "BE1"	75	12.4	208	19.4	19.0	21.1
Bentheimer "BH1"	72	13.7	2676	22.1	11.9	9.6
Fontainebleau "FB2"	80	8.1	304	11.9	48.7	9.6
Clashach "CL2"	73	8.8	426	14.1	36.1	10.2

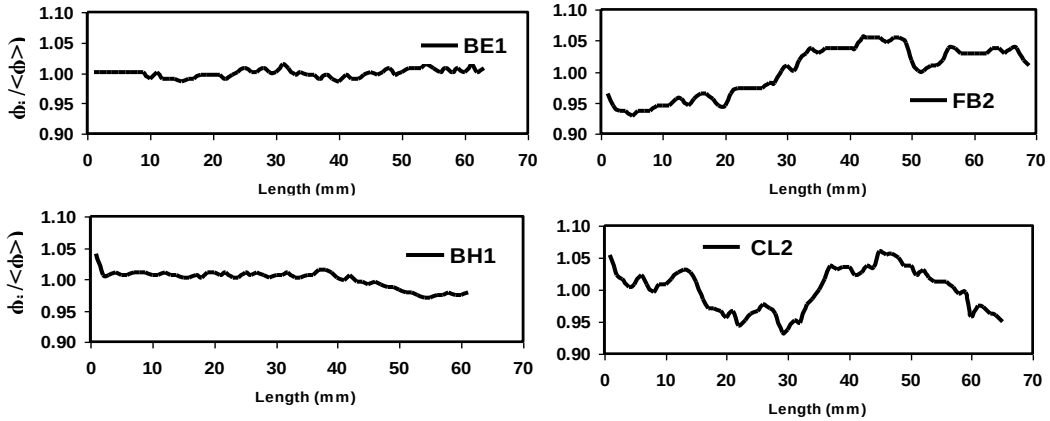

Figure 1 Normalized porosity profiles calculated by CT-scan method for the four studied sandstones: Berea (BE1), Bentheimer (BH1), Fontainebleau (FB2) and Clashach (CL2).

A mercury porosimetry test was performed on end pieces taken from samples. Figure 2 shows the pore throat radii distributions for all samples. Mean pore throat radii seem to be correlated with absolute brine permeabilities reported in Table 1.

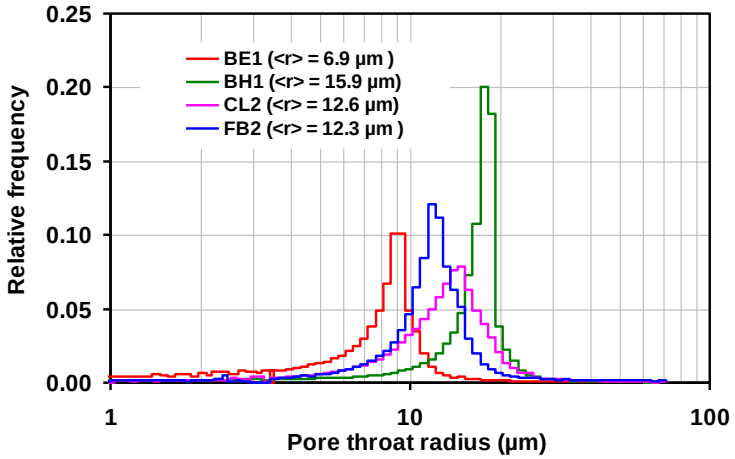

Figure 2 Pore throat radii distributions obtained by porosimetry mercury.

Core scale experiments

To determine the capillary desaturation curve, each core sample was submitted to the following sequence. The sample was vacuum saturated with KI brine for 16h and scanned before being spun under n-Decane in a centrifuge at 2000 rpm for 24h. The centrifugation produces a maximum capillary pressure of 2.5 bars at the entry of core. A porous ceramic was placed at the end of each sample to avoid capillary end effect. After determination of the irreducible water saturation value (S_{wi}) by CT scanning method (cf. Table 1), the coated cores were partially immersed in vertical position into a recipient filled with brine for several days at room temperature. The top face of the sample was covered with n-Decane to avoid drying effect. As only the lower face of the core was in contact with the brine, samples undergo a co-current spontaneous imbibition. Core plugs were then sealed in a specially designed x-ray transparent core holder and connected to a syringe pump that can deliver a flow rate between 1 cc/hr and 499 cc/hr. All displacement experiments were conducted at a temperature of 22 °C and a relative pore pressure of 1 bar. Different injection sequences were planed (cf. Table 2). First brine was injected at different flow rates from low to intermediate capillary numbers (10^{-8}-10^{-6}). Then, cores were flooded with surfactant at increasing flow rate to cover intermediate to high capillary number range. After each injection stage, the cell was disconnected and isolated for CT-scan measurement. The flow rate was maintained constant until stabilization of saturation. Fluid injections were realized from bottom to top. Total trapping number (N_t) was introduced to combine capillary and Bond effect [17]; it is expressed by the following equation:

$$N_t = N_c + N_b \quad \text{.....(1)}$$

where N_c and N_b are respectively capillary number and Bond number expressed by:

$$N_c = \frac{V\,\mu}{\sigma \cos\theta} \quad \text{.....(2)}$$

$$N_b = \frac{\Delta\rho\, g\, K_a K_{rw}}{\sigma \cos\theta} \quad \text{.....(3)}$$

where V and μ are respectively the Darcy (superficial) velocity and viscosity of the displacing fluid, σ is the interfacial tension and θ is the contact angle, $\Delta\rho$ is the density difference, g is the gravity acceleration, K_a is the single phase permeability (absolute permeability) and K_{rw} is the displacing fluid relative permeability.

Pore scale description

Four mini-plugs were extracted from end pieces of the described cores in section 1. They were 5.9 mm in diameter and 6 mm in length. The samples were coated with 0.5 mm thick epoxy resin. As in the coreflood experiment, we have used potassium iodide brine and n-Decane. The mini-plugs were submitted to drainage under n-Decane in a centrifuge at 10000 rpm for 2 hours, followed by a free spontaneous imbibition for one day. All samples were imaged into MCT equipment (Nanotom from PHOENIX) at dry and residual oil saturation conditions. Reference volumes of 1000x1000x1000 voxels have been reconstructed with 3 µm resolution (volumes reconstructed at dry state). The obtained 3D images were coded in 16 bits unsigned and have been transformed into 8 bits by linear relationships. Porous structure statistics data for all samples were determined using the pore extraction methodology described in [18]. Different structural parameters were computed: pore radii, pore throat radii, pore to throat aspect ratio.

3D volume reconstruction at residual oil saturation conditions permitted to determine oil blobs volume distribution for each sample. Registration module of Avizo was used to retrieve exactly the same region of interest in two consecutive scans.

EXPERIMENTAL RESULTS

Capillary desaturation curves

Table 2 lists residual oil saturation (Sor) results obtained at different injection steps (waterflooding (WF) and surfactant injection (SI)) and the corresponding dimensionless numbers N_c, N_b (calculated from equations (2) and (3)). Residual oil saturation (Sor) profiles as a function of trapping number (N_t) obtained in vertical flow experiments in the four sandstone cores are illustrated in Figure 3. The two lowest trapping number values were obtained during waterflooding; the other curves correspond to SDBS surfactant injection. Bentheimer and Berea samples exhibit homogeneous profile for almost all trapping number values. However, residual oil saturation profiles obtained during waterflooding for Clashach and Fontainebleau show some heterogeneity. Those heterogeneities are generated during spontaneous imbibition and seem to be correlated with porosity profile heterogeneities represented in Figure 1. Injection of the surfactant produces, in addition to lowering the global saturation, a smoothing effect on the saturation profiles.

Table 2: Summary of dimensionless numbers and residual oil saturation measurements in cores.

	Berea BE1				Fontainebleau FB2			
Sequence	**q (cc/hr)**	**Nc**	**N_b**	**S_{or} (%)**	**q (cc/hr)**	**Nc**	**N_b**	**S_{or} (%)**
WF	10	7.6E-8	2.2E-10	48.2*	10	7.6E-8	3.2E-9	25.0*
WF	30	2.3E-7	2.4E-10	48.5	80	6.0E-7	5.4E-9	24.7
SI	4	4.8E-6	1.9E-7	36.6	10	1.2E-5	1.5E-6	23.2
SI	20	2.4E-5	4.9E-7	22.3	50	6.0E-5	2.7E-6	9.8
SI	100	1.2E-4	8.1E-7	11.0	150	1.8E-4	2.8E-6	3.2
SI	300	3.6E-4	9.8E-7	3.9	499	6.0E-4	2.9E-6	0.0
	Bentheimer BH1				**Clashach CL2**			
Sequence	**q (cc/hr)**	**Nc**	**N_b**	**S_{or} (%)**	**q (cc/hr)**	**Nc**	**N_b**	**S_{or} (%)**
WF	20	1.5E-7	3.5E-8	35.1*	10	7.6E-8	2.9E-9	38.4*
WF	200	1.5E-6	3.9E-8	34.9	80	6.0E-7	3.3E-9	38.6
SI	10	1.2E-5	6.5E-6	31.7	10	1.2E-5	1.6E-6	34.3
SI	50	6.0E-5	1.1E-5	25.4	50	6.0E-5	3.3E-6	23.3
SI	150	1.8E-4	1.6E-5	18.1	150	1.8E-4	3.9E-6	15.7
SI	300	3.6E-4	1.9E-5	12.2	300	3.6E-4	4.0E-6	10.9
SI	499	6.0E-4	2.1E-5	9.7	499	6.0E-4	4.1E-6	8.5

* Value used to normalize residual oil saturation in Figure 4 (b)

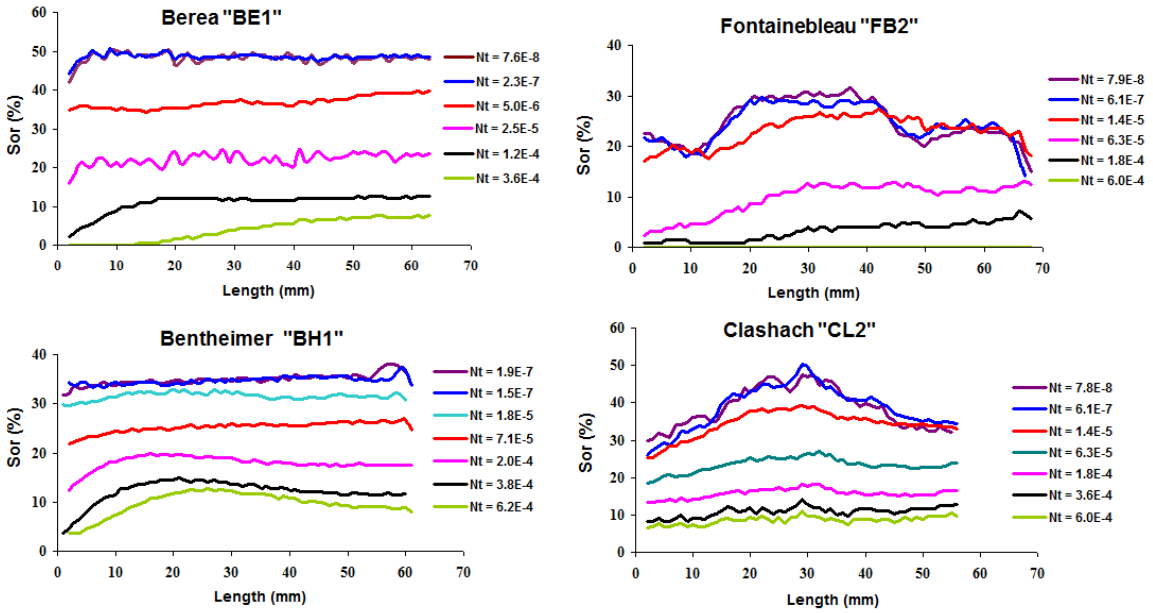

Figure 3 Residual oil saturation profiles obtained in vertical flow experiments.

Figure 4 (a and b) shows end-point brine relative permeability versus trapping number and capillary desaturation curves obtained for the four sandstones. Capillary desaturation curves were represented by normalized residual oil saturation versus trapping number. All CDCs were obtained under the same conditions; residual oil saturation mobilization occurred at trapping number values between 10^{-6} and 10^{-3}. CDC shapes are typically the same for all cores except for Fontainebleau FB1 core, exhibiting a more pronounced slop. However, we can observe a significant shift between all CDC. This dispersion, also

observed on brine relative permeability, is attributed to pore-network structure differences, since all other parameters were identical.

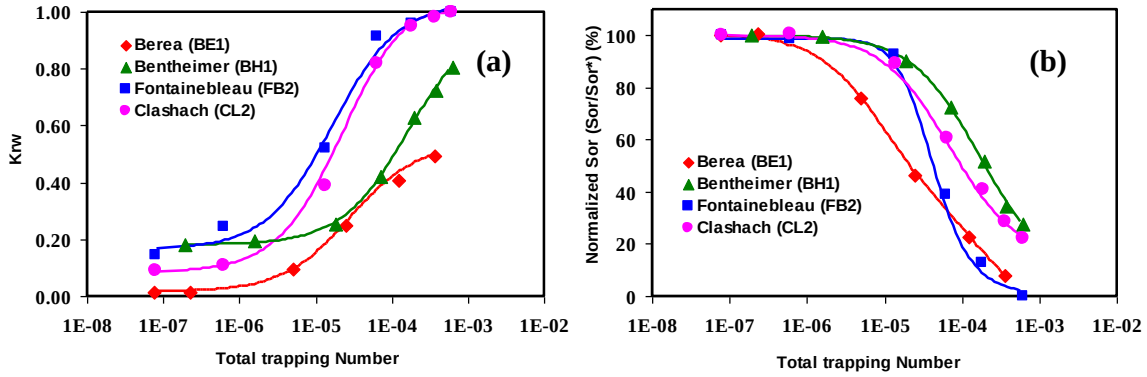

Figure 4 (a) relative brine permeabilities obtained at reached trapping number, (b) capillary desaturation curves (Sor is normalized by Sor* which is the residual oil after the first waterflood (cf. Table 2)).

Pore scale statistics

2D X-Ray density maps extracted from MCT 3D images at dry and residual oil saturation states are presented in Figure 5. At dry state, all 2D images show two main phases: quartz and void. Negligible quantities (less then 5%) of other minerals (mainly clay and iron oxide phase) can however be observed in the Clashach and Berea samples. Qualitatively Bentheimer and Berea appear to be the more porous followed by the Fontainebleau and the Clashach samples. Berea, Bentheimer, Fontainebleau and Clashach porosities estimated by segmented images method are reported in Table 3. The image-based porosities are comparable with macroscopic porosities measurements reported in Table 1 except for Clashach CL2 sandstone. The same images at residual oil saturation are represented in Figure 5. Berea, Bentheimer, Fontainebleau and Clashach residual oil saturation estimated by image segmentation are respectively 45.2 %, 45.2 %, 37.2 % and 58.2 %. For Berea sample, there is a slight difference between initial residual oil saturation estimated on macroplug and mini-plug. However, Sor estimated in other mini-plugs are higher than those obtained in macroplug especially for Clashach sandstones. A mini-plugs spontaneous imbibition were realized with two face open, which can probably create a side effect and increase residual oil saturation above the macroscopic value.

Figure 6 (a and b) shows statistic distributions of pore neck and pore body radii. The pore body radius (R) was calculated assuming a spherical pore shape. The pore neck radius (pore throat radius (r)) is the equivalent hydraulic radius, which is calculated by the ratio of pore throat cross-section area to its perimeter. The pore body radii for the different sandstones range typically between 10 µm and 160 µm. Mean pore body radius in Berea, Bentheimer, Fontainebleau and Clashach samples are respectively 28.6 µm, 36.9 µm, 41.4 µm and 38.7 µm. All samples have typically the same variation of throat radius distribution. They are narrower than pore body radius distributions. Clashach and Fontainebleau cores have typically the same mean throat radius (~13 µm); however it is slightly higher in Bentheimer sandstone (14.5 µm) and significantly lower in Berea sandstone (10.5 µm). Mean throat radii almost correlate with absolute brine

permeabilities for all samples except for Clashach sample. This discrepancy is probably due to the low porosity of the imaged sample compared to the macroscopic porosity.

Mean throat radii calculated from images are comparable to those obtained by mercury porosimetry (cf. Figure 2) except for Berea sandstone which is slightly higher. This difference can be attributed to a limitation of resolution that shifts the mean value towards higher value. The aspect ratio (R/r) was calculated by dividing pore radius by each connected throats radius, for all samples (R/r) ranges between 1 and 20 with a mean value of approximately 5 (Figure 6 (c)).

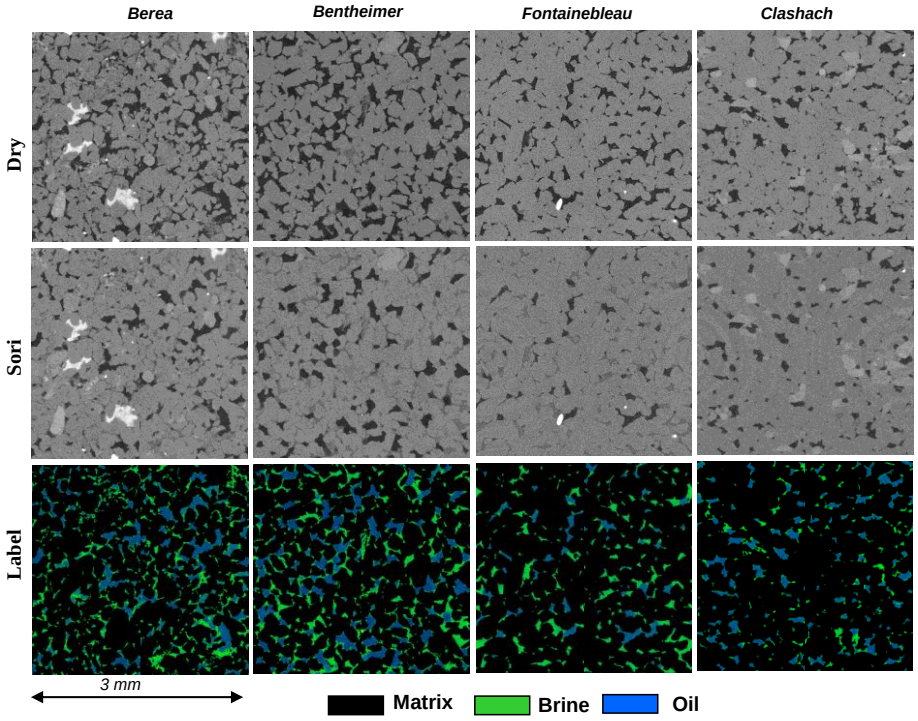

Figure 5 2D X-Ray density maps for four sandstones at dry state and residual oil saturation state.

Experimental oil blobs equivalent radii distributions for all samples obtained after free spontaneous imbibition step are reported in Figure 6 (d). An Avizo module is used to identify disconnected oil blobs, their volumes and their space positions. The blob equivalent length was calculated assuming that blob shape is equivalent to spherical volume and its length is equal to sphere diameter (d_b). Figure 6 (d) shows that blobs equivalent radius is most frequently between 10 and 50 µm. All oil blobs equivalent radius distributions show a decreasing exponential trend. A low percentage of oil clusters with equivalent radius exceeding 100 microns exists for all samples. The blobs mean equivalent radius (R_b) in Berea, Bentheimer, Fontainebleau and Clashach samples is respectively 31.5 µm, 40.1 µm, 38.6 µm and 37.2 µm. These radii are comparable to mean pore body radius, indicating that the oil blobs mainly occupy one single pore body.

Mean porosities, residual oil saturation, calculated by image segmentation method, and mean pore structure data obtained by MCT experiments are summarized in Table 3.

Table 3. Statistic data of samples used in MCT experiments.

Core type	ϕ_{img} (%)	Sor_{img} (%)	R (µm)	r (µm)	R_b (µm)
Berea "BE1"	17.6	45.2	28.6	10.5	31.5
Bentheimer "BH1"	23.1	45.2	36.9	14.8	40.1
Fontainebleau "FB2"	12.0	37.2	41.4	13.0	38.6
Clashach "CL2"	10.5	58.2	38.7	12.7	37.2

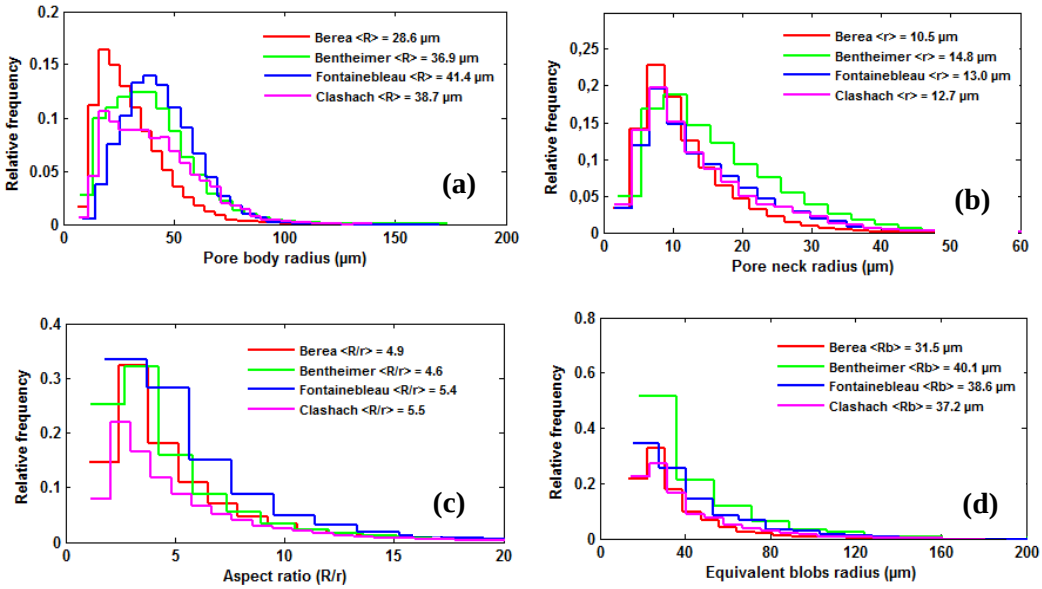

Figure 6 (a, b) pore body and pore neck radii distributions, (c) distribution of pore aspect ratio (R/r), (d) experimental distributions of equivalent blobs radius (R_b).

DISCUSSION

To understand the dispersion observed between the experimental CDCs, we have investigated the correlation between effective permeability, porous structure, oil blobs length and capillary desaturation curve. MCT showed clearly significant differences of pore structure and oil blobs length between the four sandstones. Combined effect of these parameters in fluid transport can create a significant dispersion on CDC. However, the difficulty is to determine the quantitative relationship between residual oil saturation and these parameters at core scale. In fact, we can relate rock structure to experimental data of effective brine permeability obtained at different trapping number values to upscale CDC.

Figure 7 shows a 3D view of trapped oil blobs extracted from Clashach sample at residual oil saturation and a schematic depiction of an equivalent oil blob of a length L trapped in a single pore of radius R. The pore is oriented in vertical direction. In the pore, pressure and gravity forces act towards mobilization of the oil blob through the pore throat of radius r, while capillary forces resist to mobilization.

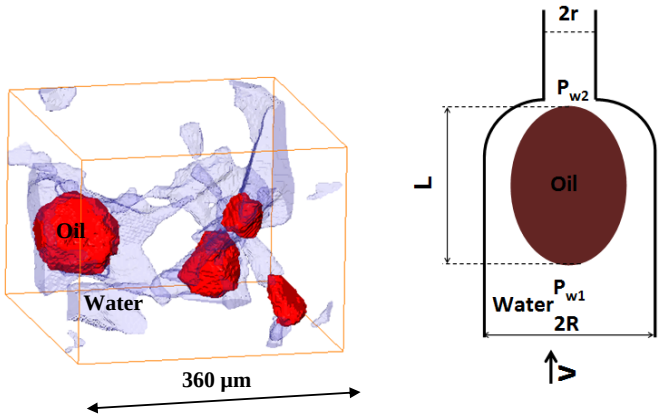

Figure 7 3D view of trapped oil blobs extracted from Clashach sample and the equivalent pore model scheme.

The minimum pressure drop (ΔP_{min}) required to mobilize oil blob is equal to the capillary pressure as expressed by equation (4):

$$(\Delta P_{min} = P_{w1} - P_{w2} - \rho_o gL) = 2\sigma \cos\theta \left(\frac{1}{r} - \frac{1}{R}\right) \quad ....(4)$$

where σ is the interfacial tension, θ is the contact angle (we assume that the receding and advancing contact angle values are the same), ρ_o is the oil density and g is the gravity acceleration. Darcy law is expressed by equation (5):

$$V = -\frac{K_a K_{rw}}{\mu L}(P_{w2} - P_{w1} + \rho_w gL) \quad .....(5)$$

where *V*, μ and ρ_w are respectively the velocity, viscosity and density of the displacing fluid. Substituting (P_{w1}-P_{w2}) deduced from equation (5) into equation (4) leads to:

$$\frac{V\mu}{\sigma \cos\theta} + \frac{(\rho_w - \rho_o)gK_a K_{rw}}{\sigma \cos\theta} = \frac{2K_a K_{rw}}{L}\left(\frac{1}{r} - \frac{1}{R}\right) \quad .....(6)$$

Using the definition of the trapping number from equation (1) and considering 1/r >> 1/R equation (6) becomes:

$$N_t = \frac{2K_a K_{rw}}{rL} \quad .....(7)$$

This equation shows that the capillary number is correlated to three main parameters: the effective permeability to water, the throat radius of the trapping pores and the trapped phase size. However, these three parameters are not independent. Indeed, the effective permeability depends on the available path that is controlled at the pore scale by the throat radius and the blocking oil cluster. It is also obvious that during a capillary desaturation process the mean size of the trapped oil cluster changes. As a consequence the quantification of these three parameters is needed for each injection step to correctly correlate the capillary number.

If we assume that fluid flow is controlled by the largest accessible pore throat radius during oil mobilization, this throat radius can be approximated by the square root of the effective brine permeability ($K_{w,eff} = K_a K_{rw}$). Then equation (7) can be written as:

$$\frac{N_t}{\sqrt{K_a K_{rw}}} = \frac{C}{L} \quad \text{.....(8)}$$

where C is a constant independent of the pore structure. When normalized residual oil saturation is plotted as a function of $N_t/\sqrt{(K_a K_{rw})}$(cf. Figure 8) less shift is observed between CDCs. According to the equation (8), the remaining of this dispersion could be due to the oil blobs length variation during the desaturation process. To validate this assumption further pore scale observations are needed to quantify the evolution of blob size as function of trapping number.

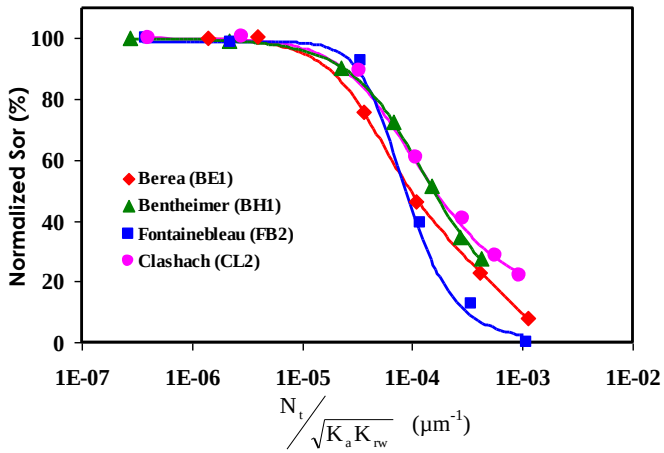

Figure 8 Capillary desaturation curves as a function of the modified trapping number.

CONCLUSIONS

The main conclusions of this study are:

- CT-scan imaging is a good tool to measure accurate CDC, and access information about local residual oil saturation variation with time and space. It also allows an estimation of local core heterogeneities and macroscopic residual oil efficiency.
- Berea, Bentheimer, Fontainebleau and Clashach sandstone coreflood experiments investigated in this work showed dispersion in shape and shift between results of normalized residual oil saturation versus trapping number. A modified trapping number was introduced that takes into account effective brine permeability, or in other words the size of the effective pathways through which fluid flow occurs. Use of the modified trapping number permits to reduce CDC dispersion.
- Capillary desaturation curves obtained in vertical flow experiments for various sandstones constitute a data set to EOR simulation.
- Oil blobs size distributions determined by MCT constitute important data which, combined to porous structure data, can be used to develop predictive modeling of CDC.

ACKNOWLEDGEMENTS

We thank IFP Energies nouvelles for permission to publish this paper. We would like to acknowledge M.C. Lynch and E. Rosenberg for their contributions in CT and µ-CT scan experiments. We gratefully acknowledge F. Lamy for his technical assistance in core floods experiments.

REFERENCES

[1] Thomas, S., Enhanced oil recovery: An overview, IFP International Conference, Lyon, vol. 63, no 1, 2008.

[2] Chatzis, I., Kuntamukkula, M., and Morrow, N., Effect of capillary number on the microstructure of residual oil in strongly water-wet sandstones, SPEJ., vol. 3, no. 3, pp. 902-912, 1988.

[3] Stegemeier, G., Mechanisms of entrapment and mobilization of oil in porous media, D.O. Shah and R.S. Schechter, Editors, Improved Oil Recovery by Surfactant and polymer Flooding, Academic Press, Inc.,New York, pp. 55–91, 1977.

[4] Delshad, M., Najafabadi, N.F., Anderson, G.A., Pope, G.A., and Sepehrnoori, K. 2009. Modeling Wettability Alteration by Surfactants in Naturally Fractured Reservoirs. SPE Res Eval & Eng 12 (3): 361-370.

[5] Abrams, A., Influence of fluid viscosity, interfacial-tension, and flow velocity on residual oil saturation left by waterflood, SPEJ, vol. 15, no. 5, pp. 437-447, 1975.

[6] Chatzis, I., and Morrow, N., Correlation of capillary number relationships for sandstone, SPEJ, vol. 24, no. 5, pp. 555-562, 1984.

[7] duPrey, E. J. L., Factors affecting liquid-liquid relative permeabilities of a consolidated porous medium, SPEJ, vol. 13, pp. 39-47, 1973.

[8] Foster, W., A low-tension waterflooding process, Journal of Petroleum Technology, vol. 13, pp. 205-210, 1973.

[9] Moore, T., Slobod, R., and Co, T. A. R., Displacement of oil by water-effect of wettability, rate, and viscosity on recovery, SPE 502, Fall Meeting of the Petroleum Branch of AIME, New Orleans, Louisiana, 2-5 October 1955.

[10] Moore, T., and Slobod, R., The effect of viscosity and capillarity on the displacement of oil by water, Producers Monthly, vol. 20, no. 10, pp. 20-30, 1956.

[11] Morrow, N., Interplay of capillary, viscous and buoyancy forces in the mobilization of residual oil, Journal of Canadian Petroleum Technology, vol. 18, no. 3, pp. 35-46, 1979.

[12] Taber, J., Dynamic and static forces required to remove a discontinuous oil phase from porous media containing oil and water, SPEJ, vol. 9, pp. 3-12, 1969.

[13] Dullien, F. A. Dhawan, G. K., Gurak, N., and Babjak, L., 1972: A relationship between pore structure and residual oil saturation in tertiary oil recovery in a water-wet system, SPEJ 12, 289-296.

[14] Zhou, D., and Stenby, E. H., Displacement of trapped oil from water-wet reservoir rock. Transport in Porous Media, 11:1-16, 1991.

[15] Land, C. S., Calculation of Imbibition Relative Permeability for Two- and Three-Phase Flow From Rock Properties, SPEJ., vol. 8, no. 2, pp. 149-156, 1968.

[16] Funk, F. F., and Withjack, E. M., Siddiqui, M., Al-Enezi, M. and Caliskan, S., Core imaging –twenty five years of equipment, techniques, and applications of x-ray computed tomography (CT) for core analysis, Society of Core Analysts held in Austin, Texas, USA 18-21 September, 2011.

[17] Pennell, K., Pope, G., and Abriola, L., Influence of viscous and buoyancy forces on the mobilization of residual tetrachloroethylene during surfactant flushing, Environmental Science & Technology, vol. 30, no. 4, pp. 1328–1335, 1996.

[18] Youssef, S. Rosenberg, E., Gland, N., Bekri, S., and Vizika, O., Quantitative 3D characterisation of the pore space of real rocks: improved µ-CT resolution and pore extraction methodology, Int. Sym. of the Society of Core Analysts, Calgary, Canada (2007).